

# Scattering of an electronic wave packet by a one-dimensional electron-phonon-coupled structure

C. Brockt\* and E. Jeckelmann

Leibniz Universität Hannover, Institut für Theoretische Physik, Appelstrasse 2, D-30167 Hannover, Germany

(Dated: June 10, 2022)

We investigate the scattering of an electron by phonons in a small structure between two one-dimensional tight-binding leads. This model mimics the quantum electron transport through atomic wires or molecular junctions coupled to metallic leads. The electron-phonon coupled structure is represented by the Holstein model. We observe permanent energy transfer from the electron to the phonon system (dissipation), transient self-trapping of the electron in the electron-phonon coupled structure (due to polaron formation and multiple reflections at the structure edges), and transmission resonances that depend strongly on the strength of the electron-phonon coupling and the adiabaticity ratio. A recently developed TEBD algorithm, optimized for bosonic degrees of freedom, is used to simulate the quantum dynamics of a wave packet launched against the electron-phonon coupled structure. Exact results are calculated for a single electron-phonon site using scattering theory and analytical approximations are obtained for limiting cases.

PACS numbers: 71.10.Fd, 72.10.-d, 71.38.Ht, 63.20.kd

## I. INTRODUCTION

The interaction between electrons and phonons plays an important role for the dynamical properties of solids, in particular for their electronic transport [1–3]. An electron moving through a vibrating lattice can dissipate its energy, be scattered off course, or become dressed by a cloud of phonons, giving rise to a quasiparticle called a polaron. These effects are very strong in low-dimensional systems such as atomic wires [4–7] and molecular junctions [8–10]. Two very recent studies [11, 12] have also demonstrated the realization of polaronic physics in Bose-Einstein condensates of ultracold atomic gases. Thus various fields of physics would benefit from a better understanding of the nonequilibrium dynamics of particles coupled to bosonic degrees of freedom.

The problem of interacting electrons and phonons out of equilibrium is too complex to be solved analytically. Thus simplified yet nontrivial many-body models are often used to obtain insights into the physics of these systems. One model of this type is the Holstein model [13], that couples tight-binding electrons linearly to quantum harmonic oscillators, which describe the lattice vibrations. The equilibrium properties of this model are relatively well understood but studying its nonequilibrium dynamics remains a challenge, which has attracted much attention recently [14–21]. Indeed, strongly fluctuating bosonic degrees of freedom make analytical and even numerical studies cumbersome, due to the large Hilbert space dimension that must be taken into account.

In this work we use a newly developed method [22] that combines the time-evolving block-decimation algorithm (TEBD) [23] with a local basis optimization (LBO) [24] to simulate an electronic wave packet scattering off a phonon structure. In previous studies, electronic wave packets were directly injected into electron-phonon coupled (EPC) chains [14, 16]. Here the EPC structure is modelled by a Holstein-type chain and is attached to long

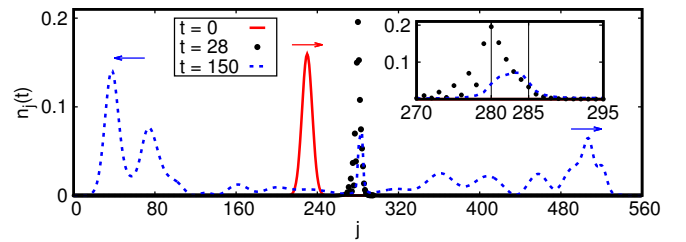


FIG. 1. (Color online) The electronic density distribution calculated with TEBD-LBO for a 6-site EPC wire with phonon frequency  $\omega_0 = 2.25t_0/\hbar$  and electron-phonon coupling  $\gamma = t_0$  at three instances of time: before (red solid line), during (black dots), and after (blue dashed line) the main scattering processes. The index  $1 \leq j \leq L = 560$  numbers the lattice sites. The red solid and blue dashed curves are multiplied by factors 2 and 10, respectively. The inset shows an enlarged view of the region around the EPC wire. Thin vertical lines show the position of the first and last EPC sites.

tight-binding leads at each end [22]. Its length varies between a single site (impurity) and up to 100 sites (wire). As shown in Fig. 1, the electronic wave packet is initially a Gaussian distribution in the left lead with a momentum toward the EPC structure, where it interacts with the phonon degrees of freedom and becomes temporarily self-trapped, and finally it is partially transmitted and reflected.

Preliminary results for this polaron scattering problem were presented in a previous work [22] to demonstrate the TEBD-LBO method. Here we extend the investigation of the rich physics offered by this simple model. We study the time evolution of the electronic wave packet coupled to the phonon degrees of freedom. A transient self-trapping of the electron on the EPC sites is observed due to polaron formation and to multiple reflections at the edges of an EPC wire. Depending on the phonon frequency and the electron-phonon coupling strength, the

wave packet can be scattered into several smaller, transmitted or reflected, wave packets with various velocities, see Fig. 1. We also study asymptotic expectation values like the reflection and transmission coefficients and the dissipated energy (i.e., the permanent energy transfer from the electron to the phonon system). We find distinct resonances in the anti-adiabatic regime, which blur with decreasing phonon frequency and vanish in the adiabatic regime. These results can be understood using the scattering theory for one EPC impurity. For adiabatic weakly-coupled systems, the analysis can be extended to structures made of several EPC sites assuming a multiple single-site reflection ansatz.

The model and initial conditions are presented in Sec. II, a brief summary of the TEBD-LBO algorithm is given in Sec. II A, the scattering theory for one EPC site is explained in Sec. II B, and the method used to compare scattering theory and wave packet simulations is detailed in Sec. II C. Our numerical results are discussed in Sec. III A for the transmission probability, in Sec. III B for the dissipated energy, and in Sec. III C for the transient self-trapping. Finally, we conclude in Sec. IV.

## II. PROBLEM AND METHODS

We investigate a one-dimensional lattice model that consists of three parts: a small segment of  $L_H$  electron-phonon coupled sites in the middle and two non-interacting tight-binding leads of length  $L_{TB} \gg L_H$  at both sides. The Hamiltonian for the whole lattice reads

$$H = -t_0 \sum_{j=1}^{L-1} \left( c_j^\dagger c_{j+1} + c_{j+1}^\dagger c_j \right) + \sum_{j=L_{TB}+1}^{L_{TB}+L_H} \left[ \hbar\omega_0 b_j^\dagger b_j - \gamma (b_j^\dagger + b_j) n_j \right], \quad (1)$$

where  $L = L_H + 2L_{TB}$  is the total number of sites while  $b_j$  and  $c_j$  annihilate a phonon (boson) and a (spinless) fermion on site  $j$ , respectively, and  $n_j = c_j^\dagger c_j$ . The model parameters are the phonon frequency  $\omega_0 > 0$ , the electron-phonon coupling  $\gamma$  and the hopping integral  $t_0$ .

The initial state

$$|\psi(t=0)\rangle = \sum_{j=1}^L \psi_j c_j^\dagger |\emptyset\rangle_e \otimes |\emptyset\rangle_p, \quad (2)$$

is a tensor product of the phonon vacuum and an electronic Gaussian wave packet

$$\psi_j = \sqrt{\frac{a}{\sigma\sqrt{2\pi}}} e^{-\frac{a^2(j-j_0)^2}{4\sigma^2} + iKja}, \quad (3)$$

with a width  $\sigma$  sufficiently larger than the lattice spacing  $a$ . The center of the wave packet  $j_0$  is always set in the left lead at  $j_0 = L_{TB} - 10\sigma/a$ . The initial wave packet velocity  $v \approx 2\frac{t_0 a}{\hbar} \sin(Ka) > 0$  is set by the wave number  $0 < K < \pi/a$ .

Our goal is to compute the time evolution of expectation values for the state

$$|\psi(t)\rangle = \exp\left(-i\frac{Ht}{\hbar}\right) |\psi(t=0)\rangle, \quad (4)$$

such as the electronic density distribution

$$n_j(t) = \langle \psi(t) | n_j | \psi(t) \rangle, \quad (5)$$

shown in Fig. 1. The total energy

$$E = \langle \psi(t) | H | \psi(t) \rangle \approx -2t_0 \cos(Ka) \quad (6)$$

is a constant of motion. For all numerical simulations presented here, the initial variance is  $\sigma^2 = 25a^2$  and the initial wave number is  $K = \frac{\pi}{2a}$  corresponding to an initial velocity  $v \approx 2at_0/\hbar$ . Thus the average total energy is  $E \approx 0$ . This corresponds to the middle of the electronic tight-binding band  $-2t_0 \leq E \leq 2t_0$ . These parameters provide a relatively broad, fast moving, and stable initial wave packet. For all numerical data shown here, we use the energy scale  $t_0 = 1$  and a lattice spacing  $a = 1$ . In addition, we set  $\hbar = 1$  so that the time unit is  $\hbar/t_0 = 1$ .

This system is expected to behave widely differently in different parameter regimes. For instance, the phonon subsystem can react instantaneously (for  $\hbar\omega_0 \gg t_0$ ) or with significant retardation (for  $\hbar\omega_0 \ll t_0$ ) to the passage of the electron. In addition, it was previously determined that dissipation can occur only for small enough phonon frequencies [22]. As another example, the ratio  $g = \gamma/(\hbar\omega_0)$  determines how strongly the electrons are dressed dynamically by phonons [17]. Therefore, we are interested in all parameter regimes from the adiabatic limit  $\hbar\omega_0 \ll t_0$  to the anti-adiabatic limit  $\hbar\omega_0 \gg t_0$  and from the weak-coupling regime  $\gamma \ll \hbar\omega_0, t_0$  to the strong-coupling regime  $\gamma \gg \hbar\omega_0, t_0$ .

### A. TEBD-LBO

The TEBD method has proven to be a very versatile and effective numerical method for simulating the quantum dynamics (4) in one-dimensional correlated lattice systems [23]. It is based on a matrix-product-state representation of the quantum state  $|\psi(t)\rangle$ . In a recent work [22] this algorithm was extended and optimized for large local Hilbert spaces such as the ones needed to represent strongly fluctuating bosons. Instead of working in the occupation number basis (bare basis), that is defined by  $b|0\rangle_p = 0$  and  $b^\dagger b|n\rangle_p = n|n\rangle_p$ , we use the eigenbases of the single-site reduced density matrices (optimal basis) for each site [24]. The structure of the resulting matrix-product-state is sketched in Fig. 2. These optimized bases can change significantly in time [17, 22], so we have to recalculate them at every time step. This algorithm is faster than the bare basis TEBD when the number  $d_O$  of optimal states needed to represent the quantum state  $|\psi(t)\rangle$  is much smaller than the number  $d$  of required bare

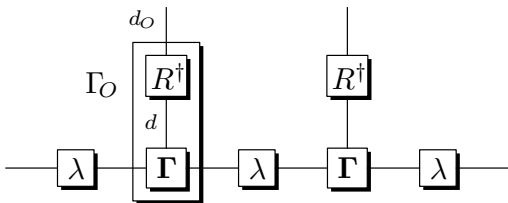


FIG. 2. Schematic representation of the matrix-product state used by the TEBD-LBO algorithm. The  $\Gamma$  matrices and the diagonal  $\lambda$  matrices have dimensions smaller or equal to  $D$  and have the same properties as in the original TEBD algorithm [23]. The matrix  $R$  describes the local transformation from the  $d$ -dimensional local bare basis to the  $d_O$ -dimensional optimized subspace.

states. In that case, the computational cost drops from  $\mathcal{O}(d^3 D^3)$  to  $\mathcal{O}(d^3 D^2)$ , where  $D$  is the bond dimension of the matrix-product-state.

In this work we have used up to  $d = 386$  bare boson states in the most difficult regime, i.e. in the adiabatic strong-coupling regime. The number of optimized boson states reaches up to  $d_O = 21$  with a cutoff of  $10^{-13}$  for the eigenvalues of the local reduced density matrix. We use separate optimized bases for a site occupied by the electron and for an empty site. (Note that for the case of one EPC impurity site, there is exactly one optimal mode in the occupied-site basis because the rest of the system is always in the vacuum state.)

We always start the TEBD simulations with the lowly entangled state (2) corresponding to  $D = 2$ . The highest bond dimension reached in the simulations presented here is  $D = 84$  with a cutoff of  $10^{-15}$  for the eigenvalues of the bipartite reduced density matrices (i.e., the squares of the diagonal elements of the matrices  $\lambda$ ). The increase of the bipartite entanglement (and thus of the necessary bond dimension  $D$ ) is mainly influenced by the length  $L_H$  of the interacting structure and the ratio  $g = \gamma/(\hbar\omega_0)$ . Thus the computational time increases faster than linear with the EPC structure size  $L_H$  because of the higher bond dimensions. (The TEBD updates for non-interacting sites take a negligible amount of time.)

We study EPC chains with up to  $L_H = 100$  sites in the weak-coupling regime (where the LBO method is not needed) and up to  $L_H = 6$  for general coupling strengths (where LBO is required), while the total system length reaches up to  $L = 580$  sites. This system length  $L$  and the maximal time  $t_{\max}$  are tuned so that reflections of the wave packets at the outer edges of the leads do not play any role. As the Gaussian wave packet always starts close to the middle of the system, the maximal time is given by  $t_{\max} \approx La/(2v) \sim 10^2 \hbar/t_0$ . We typically use a time step  $\Delta t = 5 \cdot 10^{-4} \hbar/t_0$  for the TEBD-LBO algorithm and thus  $\sim 10^5$  time steps are carried out for each simulation. The required memory is negligible (below 2 Gb) in all simulations but the CPU time, up to 150 hours for a single simulation, is a real limiting factor.

## B. Scattering theory

For the special case of a single-site EPC impurity ( $L_H = 1$ ), we can obtain some interesting information from the stationary scattering states. The stationary results should correspond to the expectation values of the Gaussian wave packets for asymptotic times  $t \rightarrow \infty$  in the limit  $L_{TB} - j_0, j_0 \gg \sigma/a \gg \pi/(Ka)$ .

We want to solve the time-independent Schrödinger equation for the Hamiltonian (1) with  $L_H = 1$ . The solution should describe an incident plane wave coming from the left with a wave number  $\pi/a > K > 0$  and being scattered by the impurity with no initial phonon excitation. After shifting the lattice indices so that the EPC impurity corresponds to  $j = 0$ , we can write a stationary scattering state as

$$|\psi\rangle_S = \sum_{j,n} \psi(j,n) |j\rangle_e \otimes |n\rangle_p, \quad (7)$$

with the (bare) phonon mode index  $n = 0, 1, \dots, \infty$  and the lattice site index  $j = -L/2, \dots, L/2$ . Far from the impurity,  $|j| \gg 1$ , the electronic state for a given number of phonons  $n$  must be a plane wave with a wave number  $k_n$  given by the energy conservation

$$E = -2t_0 \cos(Ka) = n\hbar\omega_0 - 2t_0 \cos(k_n a). \quad (8)$$

Therefore, the stationary scattering state has the form

$$\psi(j,n) = \begin{cases} Ae^{iKja} \delta_{n0} + B_n e^{-ik_n ja}, & j \leq 0 \\ C_n e^{ik_n ja}, & j \geq 0 \end{cases} \quad (9)$$

with  $k_0 = +K$  and the amplitudes of the reflected and transmitted plane waves  $B_n$  and  $C_n$ , respectively. Using the uniqueness of the wave function at  $j = 0$ , we get the conditions

$$\begin{aligned} A + B_0 &= C_0 \\ B_n &= C_n, \quad \forall n \geq 1. \end{aligned} \quad (10)$$

This implies that the amplitudes for reflected and transmitted plane waves are equal for a given number of phonon excitations  $n \geq 1$ . (This generic result agrees with our TEBD-LBO simulations for the Gaussian wave packet.) From (8) we obtain

$$k_n a = \begin{cases} \arccos\left(\frac{n\hbar\omega_0 - E}{2t_0}\right), & n < n_B, \\ i \operatorname{arcosh}\left(\frac{n\hbar\omega_0 - E}{2t_0}\right), & n \geq n_B, \end{cases} \quad (11)$$

where  $n_B \geq 1$  is defined as the smallest index  $n$  for which  $n\hbar\omega_0 > 2t_0[1 - \cos(Ka)]$ . The components (9) with  $n \geq n_B$  correspond to electronic states bound around the impurity while the components with  $n_B > n \geq 0$  correspond to scattering electronic states. Inserting (9) with (8) and (10) in the time-independent Schrödinger

equation, we obtain an infinite system of recursive linear equations

$$0 = 2i t_0 (C_0 - A) \sin(k_0 a) + \gamma C_1 \quad (12)$$

$$0 = 2i t_0 C_n \sin(k_n a) + \gamma \sqrt{n} C_{n-1} + \gamma \sqrt{n+1} C_{n+1}.$$

As the normalization of the quantum state requires that  $C_n \rightarrow 0$  for  $n \rightarrow \infty$ , we can solve these equations backwards by setting  $C_n = 0$  for all  $n$  larger than a high cutoff and then verify that the results do not depend on that cutoff. We can then calculate some stationary properties such as the transmission coefficient

$$T(K) = \sum_{n=0}^{n_B-1} \frac{\sin(k_n a)}{\sin(k_0 a)} \left| \frac{C_n}{A} \right|^2 \quad (13)$$

for an incident wave number  $K = k_0$ . For an elastic scattering process ( $n_B = 1$ ), one recovers the usual result  $T(K) = |C_0/A|^2$ .

In the anti-adiabatic limit  $\hbar\omega_0 \gg t_0$ ,  $n_B = 1$  and we can solve the equation system (12) exactly when the incident plane wave has an energy

$$E = E_m = -\varepsilon_p + m\hbar\omega_0 \quad (14)$$

with an integer  $m \geq 0$  and the polaron energy  $\varepsilon_p = \gamma^2/(\hbar\omega_0)$ . In particular, we find that

$$T(E = E_m) = \frac{4t_0^2 - E^2}{4t_0^2}. \quad (15)$$

The energies  $E_m$  are equal to the eigenenergies of the EPC impurity site when it is occupied by an electron and is disconnected from the leads. Thus the condition  $E = E_m$  corresponds to a resonant tunnelling of the incident electron with energy  $E$  through the EPC impurity.

### C. Wave packet averaging

Results such as  $T(K)$  in (13) are valid for a plane wave with a sharp wave number  $K$ . In our TEBD-LBO simulations, the initial electronic wave packet (3) is a Gaussian distribution of finite width  $\propto 1/\sigma$  around  $K$  in Fourier space. Therefore, we must average quantities such as transmission coefficients over this distribution to compare the scattering theory predictions with the TEBD-LBO data.

The discrete Fourier transform of (3) is

$$\mathcal{F}[\psi](k) = \sqrt{\sigma} \sqrt{\frac{2}{\pi}} e^{-\sigma^2(k-K)^2 - i j_0(k-K)a} \quad (16)$$

where the prefactor is chosen so that  $\mathcal{F}[\psi](k)$  is normalized if  $k$  is a continuous variable. This is justified by the fact that we consider the limit of infinitely long tight-binding leads  $L \rightarrow \infty$ . The transmission coefficient for this wave packet is then

$$T^{\text{av}}(K) = \int T(k) |\mathcal{F}[\psi](k)|^2 dk. \quad (17)$$

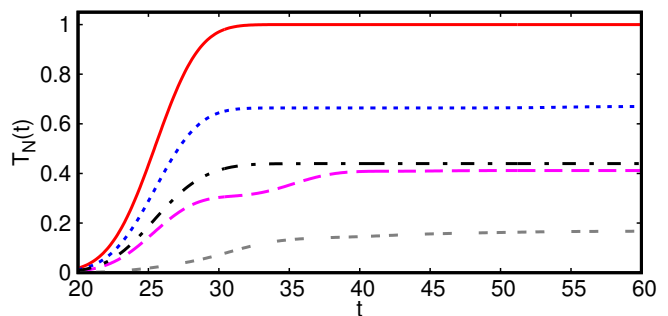


FIG. 3. (Color online) Time evolution of the numerical transmission coefficient (19) calculated with TEBD-LBO for various cases: free particle (red solid line), EPC impurity ( $L_H = 1$ ) in the adiabatic strong-coupling regime with  $\hbar\omega_0 = 0.2t_0$  and  $\gamma = 1.9t_0$  (blue dotted line) as well as with  $\hbar\omega_0 = 0.6t_0$  and  $\gamma = 3.9t_0$  (purple dashed line), and EPC structure with one site (black dashed-dotted line) and three sites (grey double-dashed line) in the intermediate regime ( $\hbar\omega_0 = 1.6t_0$  and  $\gamma = 1.85t_0$ ). The center of the wave packet reaches the first EPC site at time  $t \approx j_0 a/v \approx 25\hbar/t_0$  in all cases.

Since  $T(k)$  has to be calculated through the costly solution of the equation system for every  $k$ , we approximate this integral by a discrete sum

$$T^{\text{av}}(K) = \Delta k \sum_m |\mathcal{F}[\psi](m \Delta k)|^2 T(m \Delta k) \quad (18)$$

with intervals of length  $\Delta k = \frac{\pi}{2a} \cdot 10^{-2}$ .

## III. RESULTS

### A. Transmission

We first examine the transmission probability of an electron through the EPC structure. For TEBD-LBO simulations of Gaussian wave packets we define the transmission coefficient as the asymptotic value of the total electronic density in the right lead

$$T_N(t) = \sum_{j > L_{\text{TB}} + L_{\text{H}}} n_j(t). \quad (19)$$

We see in Fig. 3 that  $T_N(t)$  seems to converge for very long times. A similar saturation is observed for the reflected part of the Gaussian wave packet, i.e. the total density in the left lead, while the probability to find the electron in the EPC structure becomes negligibly small for long times. Therefore, we define the transmission coefficient for each simulation of a Gaussian wave packet as the value  $T = T_N(t_a)$  at some large enough time  $t_a$ . For a free wave packet ( $\gamma = 0$ ), we can estimate  $t_a \gtrsim (j_0 a + 4\sigma)/v \approx 35\hbar/t_0$  but for interacting systems the required times become longer as shown in Fig. 3. This is due to a transient self-trapping of the electron in the EPC structure, which is discussed in Sec. III C.

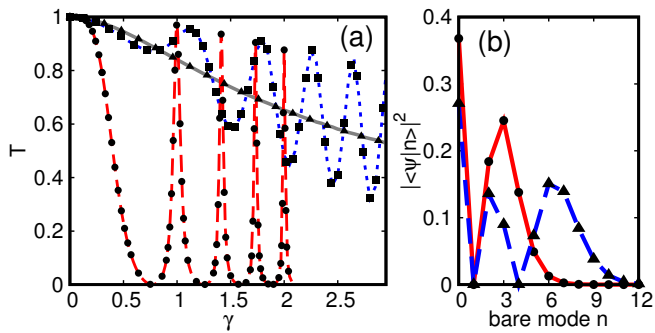


FIG. 4. (Color online) (a) Transmission coefficients calculated using TEBD-LBO (lines) and with scattering theory and wave packet averaging (symbols) for an EPC impurity ( $L_H = 1$ ). Results are plotted as a function of the electron-phonon coupling  $\gamma$  for the adiabatic regime  $\hbar\omega_0 = 0.4t_0$  (grey solid line and triangles), the intermediate regime  $\hbar\omega_0 = 1.35t_0$  (blue dotted line and squares), and the anti-adiabatic regime  $\hbar\omega_0 = 10t_0$  (red dashed line and dots). For  $\hbar\omega_0 = 10t_0$ ,  $\gamma$  is divided by a factor 10. (b) Components  $|\langle n|\psi\rangle|^2$  of the occupied-site optimal mode  $|\psi\rangle$  in the bare boson basis  $|n\rangle$  calculated with TEBD-LBO for  $\hbar\omega_0 = 10t_0$  and  $\gamma = \hbar\omega_0$  (red solid line) as well as  $\gamma = \sqrt{2}\hbar\omega_0$  (blue dashed line). Also shown are the first (circles) and second (triangles) excited states of the single-site Holstein model occupied by one electron.

In Fig. 4(a) we compare this quantity  $T$  with the transmission coefficient (18) obtained using the scattering theory and the wave packet averaging for an EPC impurity. Both approaches agree perfectly for all parameter regimes. This confirms not only the validity of the transmission coefficients calculated using (19) but also the overall accuracy of the TEBD-LBO simulations.

In the anti-adiabatic regime, we see clear transmission resonances and blockades as a function of the electron-phonon coupling strength  $\gamma$  in Fig. 4(a). The positions of the peaks agree perfectly with the resonance condition (14). Indeed, the (average) energy of the incident electron is  $E = 0$  and thus Eq. (14) yields the condition  $\gamma = \sqrt{m}\hbar\omega_0$  with  $m = 0, 1, \dots, \infty$ .

As mentioned above, for a single-site EPC structure the local reduced density matrix has only one eigenstate with finite weight when the impurity is occupied by the electron. While in general this optimal mode changes during time, we have found that it is practically constant during the whole simulation of the scattering process in the anti-adiabatic regime. At the transmission peaks this quasi-stationary mode is essentially an eigenstate of the EPC impurity disconnected from the leads, i.e. the single-site Holstein model occupied by one electron. The Hamiltonian corresponds to a shifted harmonic oscillator and its eigenstates are coherent states with the eigenenergies (14) [17]. Thus the optimal mode for the occupied impurity is the eigenstate with energy  $E_m = 0$ . This is shown explicitly in Fig. 4(b), which compares the TEBD-LBO optimal modes and the Holstein model eigenstates in the bare phonon basis for the peaks at  $\gamma = \hbar\omega_0$  (first

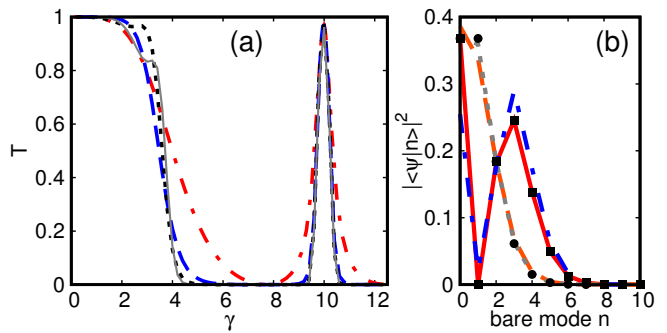


FIG. 5. (Color online) (a) Transmission coefficients calculated with TEBD-LBO in the anti-adiabatic regime ( $\hbar\omega_0 = 10t_0$ ) as a function of the electron-phonon coupling  $\gamma$  for several EPC wire lengths:  $L_H = 1$  (red dashed-dotted line),  $L_H = 2$  (blue dashed line),  $L_H = 3$  (black dotted line) and  $L_H = 4$  (grey solid line). (b) Components  $|\langle n|\psi\rangle|^2$  of the two most important optimal modes  $|\psi\rangle$  for a site occupied by an electron in the bare boson basis  $|n\rangle$  calculated with TEBD-LBO for  $L_H = 2$  and  $\hbar\omega_0 = \gamma = 10t_0$  at two points in time: First (red solid line) and second (orange dashed line) optimal modes at  $t = 25\hbar/t_0$  and first (gray dotted line) and second (blue dashed-dotted line) optimal modes at  $t = 75\hbar/t_0$ . Also shown are the ground state (circles) and first excited state (squares) of the single-site Holstein model occupied by one electron.

excited state  $m = 1$ ) and  $\gamma = \sqrt{2}\hbar\omega_0$  (second excited state  $m = 2$ ).

This resonance mechanism can be easily understood. As the phonon degrees of freedom are much faster than the electronic ones in the anti-adiabatic limit, they adapt instantly to the presence of an electron in the EPC structure and thus the system tunnels directly between eigenstates of the EPC Hamiltonian for fixed numbers of electrons. In an extended EPC structure this implies that the phonons follow the electron “adiabatically” (with a small constant delay) as shown in the Supplemental Material [25] for a 100-site EPC structure with  $\hbar\omega_0 = 2.9$  and  $\gamma = 0.25$ .

For smaller phonon frequencies, we find smaller oscillations of the transmission coefficient as a function of the electron-phonon coupling  $\gamma$ , with vanishing amplitudes in the adiabatic limit, as shown in Fig. 4(a). The position of the extrema of the transmission coefficients can no longer be predicted from the Holstein model eigenenergies. As phonons do no longer relax instantly when the electron moves, the optimal mode for the occupied impurity evolves in time but may still approach one of the Holstein model eigenstates for a finite period of time. In addition, for smaller phonon frequencies dissipation becomes possible (see the next Section) and Eq. (10) implies that reflection and transmission are equally probable when energy is transferred to the phonon degrees of freedom. Thus we expect that  $T \rightarrow \frac{1}{2}$  in the strong-coupling adiabatic limit.

This study can be extended to EPC wires. Figure 5(a) shows that the transmission coefficient has a similar behaviour for different wire lengths  $L_H$  in the anti-adiabatic

regime. Note that transmission coefficients are slightly but systematically underestimated with increasing length  $L_H$  because the probability increases that the electron is still trapped in the EPC structure when we evaluate (19). Interestingly, for weak coupling  $\gamma < \hbar\omega_0/2$  the transmission probability does not decrease systematically with increasing size of the EPC region. We see in Fig. 5(a) that the largest transmission coefficient is reached for each wire length at some coupling  $\gamma$ . We have no explanation for this surprising increase of the transmission with the EPC structure length.

The optimal modes are more involved for  $L_H > 1$  than for an impurity site. First, the local reduced density matrix for an EPC site occupied by an electron contains more than one eigenstate with a finite weight. Thus both the optimal modes and their weights can evolve with time. At the transmission resonances of the anti-adiabatic limit, however, the most important occupied-site optimal modes seem again to approximate eigenstates of the single-site Holstein model. Yet their relative weights vary strongly during the scattering process.

For instance, in the strong-coupling anti-adiabatic limit the eigenenergies of the two-site Holstein model with one electron are approximately given by

$$E_{m,n} = E_m + n\hbar\omega_0 \quad (20)$$

where  $E_m$  is the energy (14) of the site occupied by the electron and the second term is the energy of the empty site. Thus for  $\hbar\omega_0 = \gamma \gg t_0$  the resonance condition  $E_{m,n} = E = 0$  yields either the ground state of the occupied site ( $m = 0$ ) with an excited empty site ( $n = 1$ ) or the first excited state of the occupied site ( $m = 1$ ) with the empty site in its ground state (the bare phonon vacuum state  $n = 0$ ). Figure 5(b) compares the two lowest eigenstates of the single-site Holstein model with the two most important occupied-site optimal modes at two points in time for  $\hbar\omega_0 = 10t_0$  and  $\gamma = 10t_0$ . At the start of the scattering process ( $t = 25\hbar/t_0$ ), the most important optimal state matches the first excited state of the Holstein model ( $m = 1$ ) while the second most important optimal state approximates the ground state of the Holstein model ( $m = 0$ ). After the scattering process is mostly completed ( $t = 75\hbar/t_0$ ), however, the two most important optimal states have swapped their positions.

Therefore, in the anti-adiabatic regime we can understand the resonance positions and identify the most important optimal states for  $L_H > 1$  like for an EPC impurity but we cannot predict the time evolution of the weights of these optimal modes. Outside the anti-adiabatic regime, however, we cannot explain the (weaker) resonances and we have usually not been able to identify the optimal modes.

Apart from the small region seen in Fig. 5(a), the reflection is always larger for longer EPC structures. This is expected because the fraction of the electronic wave packet that is transmitted through the first site of the EPC wire can be reflected by the next one and so forth. In the weak-coupling adiabatic regime, the transmission

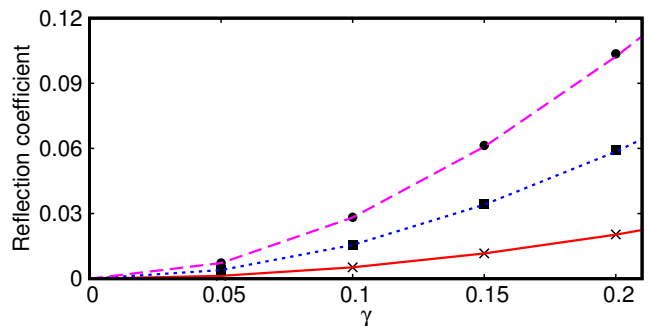


FIG. 6. (Color online) Reflection coefficient  $R(L_H)$  calculated with TEBD-LBO as a function of the electron-phonon coupling  $\gamma$  in the weak-coupling adiabatic regime ( $\hbar\omega_0 = 0.6t_0$ ) for EPC wires of length  $L_H = 2$  (crosses),  $L_H = 6$  (squares), and  $L_H = 11$  (circles). The lines show the predictions of scattering theory for an EPC impurity combined with Eq. (21) for  $R(2)$  (red solid line),  $R(6)$  (blue dotted line), and  $R(11)$  (purple dashed line).

coefficient  $T(L_H > 1)$  can be understood as the result of multiple independent single-site scattering processes. We can express the reflection coefficient  $R(L_H) = 1 - T(L_H)$  of an EPC wire of length  $L_H > 1$  in terms of the reflection coefficient  $R(L_H = 1) = 1 - T(L_H = 1)$  of an EPC impurity that is obtained from the scattering theory in Sec. II B

$$R(L_H) = \frac{L_H R(1)}{1 + (L_H - 1)R(1)}. \quad (21)$$

This formula can be proven by induction. We note that for long system lengths  $T(L_H) \propto L_H^{-1}$ . Figure 6 shows that Eq. (21) reproduces the results obtained with TEBD-LBO simulations of Gaussian wave packets for EPC structures of various lengths.

It is clear that this heuristic approach cannot hold for all parameter regimes because we assume a constant impurity transmission coefficient  $T(1) = 1 - R(1)$ , but its value (13) is only valid if the initial phonon state is the vacuum. After multiple scattering of the electron, however, we expect that the phonon degrees of freedom have become excited and thus  $T(1)$  will change and no longer be equal to (13). Therefore, Eq. (21) is valid only if the phonon state changes very slowly and very little, i.e., in the weak-coupling adiabatic limit.

Outside the anti-adiabatic regime or the weak-coupling regime, the computational effort required to compute the transmission coefficients increases quickly with the EPC structure size  $L_H$ . This is essentially due to the increase of bipartite and local entanglement and thus to the larger matrix dimensions  $D$  and  $d_O$  required. An additional effect is the increase of the necessary simulation time  $t_a$  because the electron stays longer partially localized in the EPC structure (see Sec. III C). Therefore, our results are limited to smaller electron-phonon couplings  $\gamma$  or shorter lengths  $L_H$ . Nevertheless, all our results suggest that the transmission for  $L_H > 1$  is qualitatively similar to the

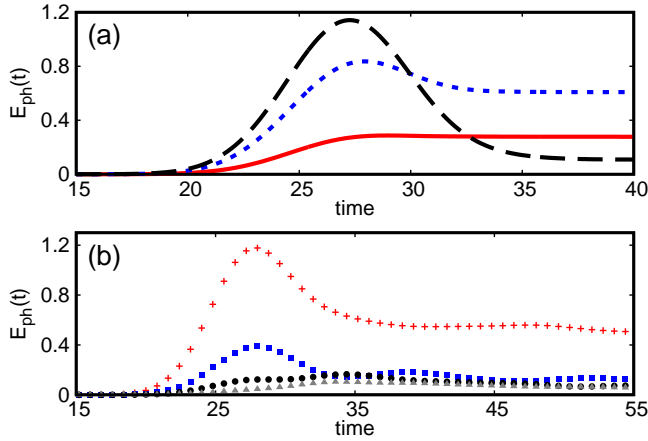


FIG. 7. (Color online) Phonon energy calculated with TEBD-LBO as a function of time. (a) For an EPC impurity with  $\hbar\omega_0 = 1.35t_0$  and three electron-phonon couplings  $\gamma = 0.8t_0$  (red solid line),  $\gamma = 1.45t_0$  (blue dotted line), and  $\gamma = 1.8t_0$  (black dashed line). (b) For a four-site EPC structure in the intermediate regime ( $\hbar\omega_0 = 1.6t_0$ ,  $\gamma = 1.85t_0$ ) the phonon energies are shown separately for the first (red crosses), second (blue squares), third (black bullets), and fourth (grey triangles) site.

transmission through an EPC impurity. For instance, the transmission coefficient for  $L_H > 1$  behaves qualitatively as shown in Fig. 4(a) as a function of the parameters  $\omega_0$  and  $\gamma$ .

### B. Dissipation

The dissipated energy  $E_D$  is the energy that is transferred permanently from the electron to the phononic degrees of freedom during the scattering process. As the electron remains only transiently in the EPC structure (see next section), the electron-phonon interaction energy vanishes for long times. Consequently,  $E_D$  is given by the loss of electronic energy or, equivalently, by the gain of phonon energy for long times. Thus we evaluate the time-dependent expectation value of the phonon energy

$$E_{\text{ph}}(t) = \hbar\omega_0 \sum_j \langle \psi(t) | b_j^\dagger b_j | \psi(t) \rangle. \quad (22)$$

Figure 7 shows that this quantity converges for very long times like the transmission coefficient (19). As the initial state (2) has no phonon energy, we define the dissipated energy for each simulation of a Gaussian wave packet as the value  $E_D = E_{\text{ph}}(t_a)$  at some large enough time  $t_a$ . Obviously, this is the same time  $t_a$  that is used to determine the transmission coefficient from (19).

Figure 7 also shows that the phonon energy  $E_{\text{ph}}(t)$  does not increase monotonically with time. The behavior of  $E_{\text{ph}}(t)$  depends strongly on the electron-phonon coupling  $\gamma$ , as illustrated in Fig. 7(a), but is also dif-

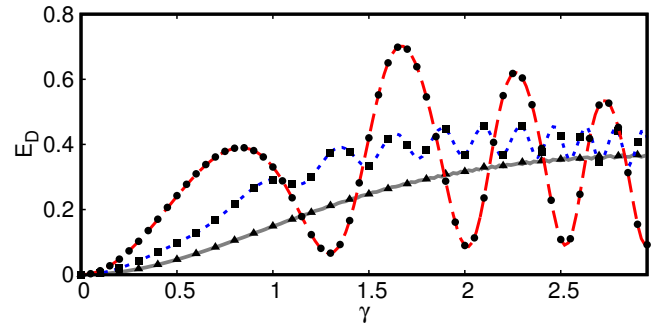


FIG. 8. (Color online) Dissipated energies calculated using TEBD-LBO (symbols) and with scattering theory and wave packet averaging (lines) for an EPC impurity ( $L_H = 1$ ). Results are plotted as a function of the electron-phonon coupling  $\gamma$  for the adiabatic regime  $\hbar\omega_0 = 0.4t_0$  (grey solid line and triangles), the intermediate regime  $\hbar\omega_0 = 0.9t_0$  (blue dotted line and squares), and close to the limit of the nondissipative regime  $\hbar\omega_0 = 1.5t_0$  (red dashed line and dots).

ferent for each site of a multi-site EPC structure, as shown in Fig. 7(b). Nevertheless the overall behavior can be understood qualitatively. Phonons are generated when the electronic wave packet reaches the EPC structure. Then we observe a maximum of  $E_{\text{ph}}(t)$  when the electron is mostly localized on EPC sites. For longer times, these phonons are annihilated when the electron leaves the EPC sites. Yet some phonons may remain permanently excited after the electron has left the EPC structure resulting in a permanent energy transfer from the electron to the phononic degrees of freedom. Consequently, partial wave packets are scattered inelastically with velocities  $v_n = v \sin(k_n a)$  that are lower than the incident velocity  $v \approx 2at_0/\hbar$  [22].

This inelastic scattering process occurs locally when the electron moves from one EPC site to the next one, as seen in Fig. 7(b). In this example, a permanent phonon is generated on the first EPC site reached by the electronic wave packet with a relatively high probability. But only transient phonons are generated on the three following EPC sites because the initial electronic kinetic energy  $2t_0$  is not high enough to generate two permanent phonons with energy  $\hbar\omega_0 = 1.6t_0$  each.

Note that the dissipated energy cannot exceed the initial excess energy of the electron. Thus phononic degrees of freedom with their minimal excitation energy  $\hbar\omega_0$  cannot be permanently excited by the electron-phonon scattering process if  $\hbar\omega_0$  is larger than this initial energy [22]. As the initial excess energy is always  $2t_0$  in our simulations of the Gaussian wave packet, there is no dissipation for phonon frequencies  $\omega_0 \geq 2t_0/\hbar$ . In particular, there is no dissipation in the anti-adiabatic regime.

Additionally, Fig. 7(a) shows that the maximal phonon energy reached during the scattering process increases monotonically with the coupling strength  $\gamma$ . In contrast, we have found that the dissipated energy varies in a complicated way with  $\omega_0$  and  $\gamma$ , as also illustrated in Fig. 8.

To shed some light on this behavior, we again examine the single-site EPC impurity in detail.

Within the scattering theory for an EPC impurity site, we assume that the dissipated energy is given by the average number of excited phonons in the scattering states

$$E_D(K) = 2\hbar\omega_0 \sum_{n=1}^{n_B-1} n \frac{\sin(k_n a)}{\sin(k_0 a)} \left| \frac{C_n}{A} \right|^2. \quad (23)$$

The factor 2 originates from the condition  $B_n = C_n$  for  $n > 0$ . As  $n_B = 1$  for  $K = \pi/(2a)$  and  $\hbar\omega_0 > 2t_0$ , we obtain  $E_D(K = \pi/(2a)) = 0$  and thus the scattering theory confirms that there is no dissipation in the parameter regime  $\hbar\omega_0 > 2t_0$ . To compare with the TEBD-LBO simulations, we have again to average the quantity (23) over the Gaussian wave packet as explained for the transmission coefficient in Sec. II C.

Figure 8 compares  $E_D^{\text{av}}(K)$  and the energy dissipation  $E_D$  calculated with TEBD-LBO for Gaussian wave packets. The perfect agreement between both approaches confirms again the accuracy of our TEBD-LBO method but also demonstrates that the definition (23) is correct for the dissipated energy within the scattering theory. For weak electron-phonon coupling we find that the dissipation increases monotonically with  $\gamma$ . We see in Fig. 8 however that the dissipated energy oscillates for larger values of  $\gamma$ , with vanishing amplitude in the adiabatic limit. This is reminiscent of the transmission oscillations in Fig. 4. Neither the extrema positions nor the oscillation frequencies (as a function of  $\gamma$ ) seem to coincide, however.

Nevertheless, in the special case  $t_0 < \hbar\omega_0 < 2t_0$  ( $\Rightarrow n_B = 2$ ), the definition (23) and the scattering theory in Sec. II B yield a simple relation between transmission coefficient  $T(K)$  and dissipated energy  $E_D(K)$  for the EPC impurity

$$E_D(K) = 2\hbar\omega_0 [1 - T(K)] \frac{\sin(Ka) \sin(k_1 a)}{\frac{\gamma^2}{4t_0^2} + \sin(Ka) \sin(k_1 a)}. \quad (24)$$

This equation demonstrates that dissipation is proportional to reflection, at least in this special case, although the dependence of both quantities on the model parameters  $\gamma$ ,  $\omega_0$ , and  $K$  is different.

As for the transmission coefficient, the TEBD-LBO study of the dissipated energy can be extended to multi-site EPC structures. Again the computational effort required to compute  $E_D$  increases quickly with the EPC structure size  $L_H$  outside the weak-coupling regime. Therefore, our results are limited to smaller electron-phonon couplings  $\gamma$  than for the EPC impurity or to short lengths  $L_H$ . Nevertheless, all our results suggest that the dissipation for  $L_H > 1$  is qualitatively similar to the dissipation through an EPC impurity. For instance,  $E_D$  behaves qualitatively as shown in Fig. 8 as a function of the parameters  $\omega_0$  and  $\gamma$ . Moreover, transmission  $T$  and dissipated energy  $E_D$  seems to be related in some complicated way, as discussed above.

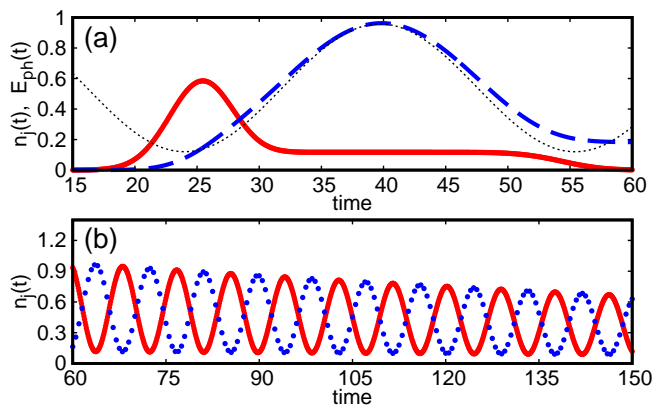


FIG. 9. (Color online) (a) Electronic density on the EPC impurity (red solid line) and phonon energy (blue dashed line) calculated with TEBD-LBO as a function of time for  $L_H = 1$ ,  $\hbar\omega_0 = 0.20t_0$ , and  $\gamma = 1.90t_0$ . The electron density is multiplied by a factor 10. The black dotted line shows Eq. (25) with  $t_{\text{off}} = 24t_0/\hbar$ ,  $E_{\text{off}} = 0.12t_0$ , and a constant average density  $n_j(t = 40\hbar/t_0) = 0.0116$ . (b) Electronic densities (multiplied by a factor 100) calculated with TEBD-LBO as a function of time on the left (red line) and right (blue dots) sites of a two-site EPC structure with  $\hbar\omega_0 = \gamma = 10t_0$ .

### C. Transient self-trapping

In a preliminary study [22], we reported that a fraction of the electronic wave packet could become temporarily self-trapped in the EPC structure and then be belatedly transmitted or reflected. We have verified that this transient self-trapping is quite common in the scattering problem discussed here, although it does not occur for all values of the model parameters. For instance, it is responsible for the occurrence of plateaus in the time-dependent transmission coefficients for some (but not all) model parameters, as seen in Fig. 3. Below we examine some aspects of this phenomenon more closely.

Figure 9(a) shows a clear example of the transient self-trapping of the electron. The electronic density measured on the EPC impurity reveals that the wave packet reaches it at time  $t \approx 20\hbar/t_0$ , then most of the electronic wave packet has left the EPC site by  $t \approx 30\hbar/t_0$  but a small fraction remains there up to  $t \approx 50\hbar/t_0$ . The first time scale corresponds simply to the passage of the Gaussian wave packet over the EPC site with negligible scattering and is set by the wave packet width  $\sigma$  and velocity  $v$  (see Sec. II).

The second time scale is due to the trapping of the electron by the effective on-site potential that its presence has induced. The self-trapping time scale ( $\Delta t \approx 30\hbar/t_0$ ) seems to be related to the period of the phonon degrees of freedom,  $\frac{2\pi}{\omega_0} = 10\pi\hbar/t_0$ . During that time interval the phonon system behaves like in the single-site Holstein model occupied by one electron, i.e., like a coherent state in a shifted harmonic oscillator. A similar behavior was found for the decay of a highly excited charge carrier in the one-dimensional Holstein model [17]. Thus one can



estimate that

$$E_{\text{ph}}(t) \approx n_j(t)2\varepsilon_p\{1 - \cos[\omega_0(t - t_{\text{off}})]\} + E_{\text{off}} \quad (25)$$

where  $n_j(t)$  is the fraction of the electron density that is currently trapped on the EPC site,  $t_{\text{off}}$  is a time offset that depends on the initial conditions (e.g.,  $t_{\text{off}} \approx j_0 a/v = 25t_0/\hbar$ ), and  $E_{\text{off}}$  is an energy offset that is related to the asymptotic phonon energy  $E_{\text{ph}}(t_a)$ . Figure 9(a) confirms that the phonon energy agrees with this equation (using fitted parameters  $t_{\text{off}} = 24t_0/\hbar$  and  $E_{\text{off}} = 0.12t_0$ ) during the transient self-trapping time. Therefore, in that time interval the system has formed a highly excited polaron (a mobile quasi-particle made of an electron dressed by a phonon cloud) as found for the decay problem in Ref. [17]. Note that the fraction of the wave packet that gets trapped,  $n_j(t)$ , depends mostly on the electron-phonon coupling strength  $\gamma$ .

In Fig. 9(a) there is a single plateau in the electronic density indicating the generation of just one delayed partial wave packet each for transmission and reflection. For longer EPC structures we found previously that several partial wave packets can be transmitted and reflected at approximately equidistant times [see Fig. 3(a) in Ref. [22]]. The transient behavior of EPC structures with  $L_H > 1$  is indeed more intricate than for a single-site EPC impurity because there is a second self-trapping mechanism besides the polaron formation. The electron induces an extended potential well in the EPC structure. Its wave function can be (partially) reflected multiple times at the edge of this potential well. Thus part of the wave packet oscillates inside the EPC structure and slowly leaks out into the leads.

This effect is illustrated in Fig. 9(b) for a two-site EPC structure at times  $t \geq 60\hbar/t_0$  when 99% of the wave packet has already been transmitted or reflected. Nevertheless, we see that a small fraction of the electronic density is still trapped inside the EPC structure and jumps back and forth between both sites with a slowly decaying amplitude. At every period  $t \approx 8\hbar/t_0$  a small wave packet is belatedly transmitted or reflected. (This indicates that the wave packet velocity is about  $\frac{t_0 a}{4\hbar}$  inside the EPC structure and thus about 8 times slower than for a free wave packet.) Due to the multiple reflections, however, the overall self-trapping time is extended greatly and it is clearly over  $\Delta t = 150\hbar/t_0$  in the example of Fig. 9(b). Finally, note that this multiple scattering at the EPC structure edges should not be confused with the multiple inter-site scattering leading to Eq. (21).

It is tempting to define an overall self-trapping time as the delay of the wave packet transmitted through the EPC structure compared to a non-interacting wave packet. For instance, one could attempt to use the distance to the rightmost maximum in the density distribution. We see in Fig. 10, however, that this definition can result in a negative self-trapping time. For transmission minima in particular, the scattered wave packet seems to be ahead of the free one. This is related to the Hartman effect [26]: the transmission time of a (Gaussian)

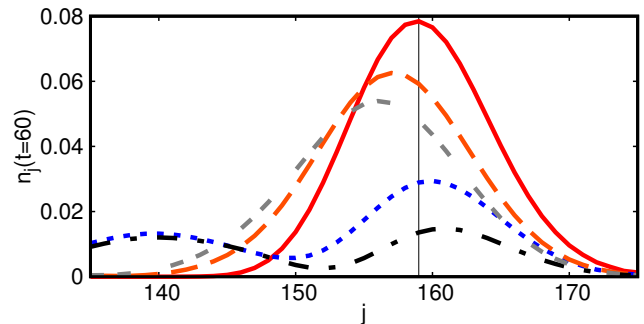


FIG. 10. (Color online) The rightmost part of the electronic density distributions  $n_j(t)$  calculated with TEBD-LBO at  $t = 60\hbar/t_0$  as a function of the lattice site index  $j$  for  $L_H = 1$ ,  $\hbar\omega_0 = 1.35t_0$  and several electron-phonon couplings corresponding to transmission minima at  $\gamma = 1.5t_0$  (blue dotted line) and at  $\gamma = 2.45t_0$  (black dashed-dotted line) as well as to transmission maxima at  $\gamma = 1.80t_0$  (orange dashed line) and at  $\gamma = 2.65t_0$  (grey double-dashed line). The vertical black line shows the position of the maximum of the free Gaussian wave packet (red line).

wave packet through a potential barrier can be shorter than the time required by a free wave packet to travel a distance equal to the barrier width. We observe a similar effect in Fig. 10 although the scattering is not caused by a static potential barrier but by dynamical degrees of freedom.

This effect reveals that one has to be careful when measuring times for quantum systems. For a wave packet tunneling through a potential barrier, it was shown that there is a trade-off between the speedup of the transmitted wave packet and the damping of its amplitude [27]. As a result, the probability for the electron to reach a certain distance before some given time is always reduced by the tunneling through a potential barrier compared to the probability for a free wave packet. Our results, as illustrated in Fig. 10, agree with Ref. [27]. Clearly, the probability of finding the electron on the right of the vertical line is larger for the free wave packet than for any of the scattered ones although the density maxima are further on the right in some cases.

In all our TEBD-LBO simulations we have never observed a permanent trapping of the electron in the EPC structure. On the one hand, this absence of localization is expected because a trapped electron cannot dissipate its energy in the present model. Any emitted phonon will be sooner or later reabsorbed if the electron remains long enough in the EPC structure and electronic energy can only be dissipated if the electron moves away in the noninteracting leads. On the other hand, one intuitively expects that the electron should progressively lose its kinetic energy to the phonons left behind and ultimately come to rest if the EPC wire is long enough, like a particle in a viscous environment. Actually, once the electronic wave packet is well inside a long EPC chain, the tight-binding leads are no longer relevant and the relax-

ation dynamics should be similar to the problem of an excited electron in the one-dimensional Holstein model, which was thoroughly investigated in Ref. [17]. Thus one expects that the kinetic energy of the electron (or the resulting polaron) should be permanently transferred to the phonon system in the adiabatic regime. Unfortunately, we have not yet been able to simulate the conditions where this could happen, i.e., long enough EPC chains, low phonon frequency, and high dissipation rate (which implies a strong enough electron-phonon coupling) because of the very high computational effort required.

#### IV. CONCLUSION

We have studied a Gaussian electronic wave packet scattering off a one-dimensional electron-phonon-coupled structure connected to tight-binding leads using the TEBD-LBO method. We have found that this simple nonequilibrium problem offers a rich physics including transmission resonances, dissipation, and transient self-trapping due to polaron formation and multiple reflections at the EPC structure edges. Many of these features can be understood qualitatively using scattering theory for a single-site EPC impurity. For asymptotic expectation values (transmission coefficients and dissipated energy), we find a perfect agreement between our numerical TEBD-LBO simulations and the exact scattering theory results. This confirms the reliability of the TEBD-LBO method even for long-time simulations. Nevertheless, further investigations are required to understand long EPC chains more thoroughly. Although we discuss only the case of an incident wave number  $K = \pi/(2a)$  in this paper, the results remain qualitatively similar for other wave numbers  $0 < K < \pi/a$ .

Our results have some implications for the effects of lattice or molecular vibrations on the quantum electronic transport through atomic wires or molecular junctions coupled to metallic leads. Indeed, if one assumes that the electrical conductance of a quantum conductor is determined by its scattering properties [28], such as the Landauer formula  $G = (e^2/h)T$  in the simplest case,

the transmission coefficients provide some information on the transport properties. In the weak-coupling adiabatic limit, we have found that  $T \sim 1/L_H$  and thus the resistance  $1/G$  increases linearly with the wire length  $L_H$ , as observed experimentally in macroscopic resistors. This is also consistent with the linear increase of the dissipated energy with the wire length in that limit. In the anti-adiabatic regime, there is no dissipation and we have found transmission resonances that do not depend significantly on  $L_H$ . In particular, at the resonances with  $T = 1$  the EPC wire is an ideal conductor. However, we also find transmission blockades  $T = 0$  corresponding to a perfect insulator. More generally, the dissipated energy and the transmission probability vary significantly and independently with the parameters  $\omega_0, \gamma$ , and  $L_H$ . Our numerical data and the exact result (24) suggest that both quantities are related but we do not understand the precise relation yet. In particular, the strict classical relation between (macroscopic) dissipation and resistance,  $E_D \propto G^{-1}$  does not seem to be always fulfilled in the present microscopic model.

Another open question is the effect of the effective interaction between electrons that is induced by the electron-phonon coupling, if more than one electron is in the EPC structure at the same time. The TEBD method can be used to determine the linear and nonlinear transport properties of interacting wires coupled to leads with a finite density of charge carriers [29]. Thus we plan to extend the present study of EPC wires to the case of finite electronic density.

#### ACKNOWLEDGMENTS

We thank Florian Dorfner, Fabian Heidrich-Meisner, Kyle Poland, and Andreas Weichselbaum for helpful discussions. We acknowledge support from the DFG (Deutsche Forschungsgemeinschaft) through grant Nos. JE 261/2-1 in the Research Unit *Advanced Computational Methods for Strongly Correlated Quantum Systems* (FOR 1807). Some calculations were carried out on the cluster system at the Leibniz Universität Hannover.

---

\* E-mail: [christoph.brockt@itp.uni-hannover.de](mailto:christoph.brockt@itp.uni-hannover.de)

<sup>1</sup> J. M. Ziman, *Electrons and Phonons: The Theory of Transport Phenomena in Solids* (Clarendon Press, Oxford, 1960).

<sup>2</sup> G. D. Mahan, *Many-Particle Physics* (Kluwer Academic Publishers, New York, 2000).

<sup>3</sup> J. Sólyom, *Fundamentals of the Physics of Solids, Volume 2 - Electronic Properties* (Springer, Berlin, 2009).

<sup>4</sup> N. Agraït, C. Untiedt, G. Rubio-Bollinger, and S. Vieira, Onset of energy dissipation in ballistic atomic wires, *Phys. Rev. Lett.* **88**, 216803 (2002).

<sup>5</sup> N. Agraït, C. Untiedt, G. Rubio-Bollinger, and S. Vieira, Electron transport and phonons in atomic wires, *Chemical*

*Physics* **281**, 231 (2002).

<sup>6</sup> H. Ness and A. Fisher, Coherent electron injection and transport in molecular wires: inelastic tunneling and electron-phonon interactions, *Chemical Physics* **281**, 279 (2002).

<sup>7</sup> J. Hihath and N. Tao, Electron-phonon interactions in atomic and molecular devices, *Progress in Surface Science* **87**, 189 (2012).

<sup>8</sup> M. Galperin, M. A. Ratner, and A. Nitzan, Molecular transport junctions: vibrational effects, *J. Phys.: Condens. Matter* **19**, 103201 (2007).

<sup>9</sup> E. A. Osorio, T. Bjørnholm, J.-M. Lehn, M. Ruben, and H. S. J. van der Zant, Single-molecule transport in three-

- terminal devices, *J. Phys.: Condens. Matter* **20**, 374121 (2008).
- <sup>10</sup> N. A. Zimbovskaya and M. R. Pederson, Electron transport through molecular junctions, *Phys. Rep.* **509**, 1 (2011).
  - <sup>11</sup> M.-G. Hu, M. J. Van de Graaff, D. Kedar, J. P. Corson, E. A. Cornell, and D. S. Jin, Bose polarons in the strongly interacting regime, *Phys. Rev. Lett.* **117**, 055301 (2016).
  - <sup>12</sup> N. B. Jørgensen, L. Wacker, K. T. Skalmstang, M. M. Parish, J. Levinsen, R. S. Christensen, G. M. Bruun, and J. J. Arlt, Observation of attractive and repulsive polarons in a Bose-Einstein condensate, *Phys. Rev. Lett.* **117**, 055302 (2016).
  - <sup>13</sup> T. Holstein, Studies of polaron motion: Part I. The molecular-crystal model, *Ann. Phys.* **8**, 325 (1959).
  - <sup>14</sup> L.-C. Ku and S. A. Trugman, Quantum dynamics of polaron formation, *Phys. Rev. B* **75**, 014307 (2007).
  - <sup>15</sup> B. Luo, J. Ye, C. Guan, and Y. Zhao, Validity of time-dependent trial states for the Holstein polaron, *Phys. Chem. Chem. Phys.* **12**, 15073 (2010).
  - <sup>16</sup> H. Fehske, G. Wellein, and A. R. Bishop, Spatiotemporal evolution of polaronic states in finite quantum systems, *Phys. Rev. B* **83**, 075104 (2011).
  - <sup>17</sup> F. Dorfner, L. Vidmar, C. Brockt, E. Jeckelmann, and F. Heidrich-Meisner, Real-time decay of a highly excited charge carrier in the one-dimensional Holstein model, *Phys. Rev. B* **91**, 104302 (2015).
  - <sup>18</sup> S. Sayyad and M. Eckstein, Coexistence of excited polarons and metastable delocalized states in photoinduced metals, *Phys. Rev. B* **91**, 104301 (2015).
  - <sup>19</sup> A. S. Mishchenko, N. Nagaosa, G. De Filippis, A. de Candia, and V. Cataudella, Mobility of Holstein polaron at finite temperature: An unbiased approach, *Phys. Rev. Lett.* **114**, 146401 (2015).
  - <sup>20</sup> N. Zhou, Z. Huang, J. Zhu, V. Chernyak, and Y. Zhao, Polaron dynamics with a multitude of Davydov D2 trial states, *J. Chem. Phys.* **143**, 014113 (2015).
  - <sup>21</sup> L. Chen, Y. Zhao, and Y. Tanimura, Dynamics of a One-Dimensional Holstein Polaron with the Hierarchical Equations of Motion Approach, *J. Phys. Chem. Lett.* **6**, 3110 (2015).
  - <sup>22</sup> C. Brockt, F. Dorfner, L. Vidmar, F. Heidrich-Meisner, and E. Jeckelmann, Matrix-product-state method with a dynamical local basis optimization for bosonic systems out of equilibrium, *Phys. Rev. B* **92**, 241106 (2015).
  - <sup>23</sup> G. Vidal, Efficient simulation of one-dimensional quantum many-body systems, *Phys. Rev. Lett.* **93**, 040502 (2004).
  - <sup>24</sup> C. Zhang, E. Jeckelmann, and S. R. White, Density Matrix Approach to Local Hilbert Space Reduction, *Phys. Rev. Lett.* **80**, 2661 (1998).
  - <sup>25</sup> See Supplemental Material at [URL will be inserted by publisher] for a movie of the time evolution of the phononic and electronic densities in the anti-adiabatic regime.
  - <sup>26</sup> T. E. Hartman, Tunneling of a wave packet, *Journal of Applied Physics* **33**, 3427 (1962).
  - <sup>27</sup> J. Kiukas, A. Ruschhaupt, and R. F. Werner, Tunneling times with covariant measurements, *Foundations of Physics* **39**, 829 (2009).
  - <sup>28</sup> Y. Nazarov and Y. M. Blanter, *Quantum transport: Introduction to Nanoscience* (Cambridge University Press, Cambridge, 2009).
  - <sup>29</sup> M. Einhellinger, A. Cojuhovski, and E. Jeckelmann, Numerical method for nonlinear steady-state transport in one-dimensional correlated conductors, *Phys. Rev. B* **85**, 235141 (2012).